JOC The Journal of Organic Chemistry

Article

pubs.acs.org/joc

Mechanisms of the $InCl_3$-Catalyzed Type-I, II, and III Cycloisomerizations of 1,6-Enynes

Lian-Gang Zhuo, Ji-Ji Zhang, and Zhi-Xiang Yu*

Beijing National Laboratory for Molecular Sciences (BNLMS), Key Laboratory of Bioorganic Chemistry and Molecular Engineering of Ministry of Education, College of Chemistry, Peking University, Beijing 100871, China

Supporting Information

ABSTRACT: $InCl_3$-catalyzed cycloisomerizations of 1,6-enynes can give either type-I dienes and cyclohexenes (type-III dienes), or type-II dienes, depending on the substitutions in the substrates. Previously, we studied how the type-II diene products were generated and found that the real catalytic species for the cycloisomerizations is $InCl_2^+$ (*J. Org. Chem.* **2012**, *77*, 8527−8540). In the present paper, we used density functional theory (DFT) calculations to reveal how the type-I and type-III dienes were generated. A unified model to explain how substituents affect the regiochemistry of type-I, II, and III cycloisomerizations has been provided. Experimental and computational investigation of the $InCl_3$-catalyzed cycloisomerization of 1,6-enynes with both substituents at the alkyne and alkene parts has also been reported in the present study.

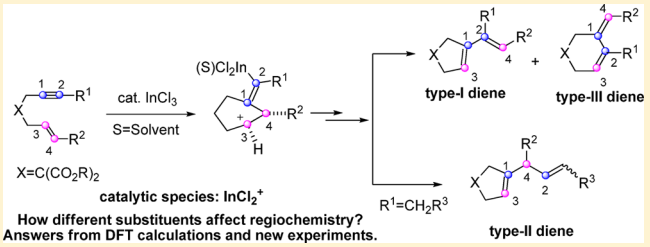

INTRODUCTION

Cycloisomerizations of 1,6-enynes catalyzed by transition metals or main group metals can give either type-I or type-II diene products, together with the type-III dienes (cyclohexenes) in some cases (Scheme 1).[1−11] Formations of the cycloisomerization products are often dependent on both the used catalysts and the substitution patterns in the substrates. For example, Chatani and co-workers found that $InCl_3$-catalyzed cycloisomerizations of **a**-**1** gave type-II nonconjugated dienes, while the reactions of **b**-**1** and **c**-**1** gave both type-I and type-III dienes (Scheme 2).[4]

We have previously studied how the type-II nonconjugated dienes (reaction 1, Scheme 2) were generated, finding that the real catalytic species in the cycloisomerization is not $InCl_3$, but is $InCl_2^+$, generated in situ (this can be understood by the net result of 1,6-enyne + 2 $InCl_3$ = 1,6-enyne-$InCl_2^+$ + $InCl_4^-$) (Figure 1).[12,13] This discovery was very important for understanding the mechanism and the encountered selectivity of conjugated versus nonconjugated [1,2]-H shift processes in this reaction. We found that the $InCl_3$-catalyzed cycloisomerization reaction starts from the coordination of $InCl_2^+$ to the alkyne part of the enyne substrate. Then nonclassical cyclopropanation, homoallylic cation rearrangement, and cation coordination assisted nonallylic hydrogen migration give the final nonconjugated type-II diene product. The preference of generating nonconjugated dienes over conjugated dienes is mainly due to the coordination of the $InCl_2^+$ to the alkene part in the [1,2]-hydride shift transition states (**a**-**TS7**-***trans*** and **a**-**TS7**-***cis***), generating a positively charged alkene. Consequently, the conjugated [1,2]-H shift (its transition state is destabilized by the positively charged alkene coordinated by the In atom) becomes disfavored compared to the nonconjugated [1,2]-H shifts since the corresponding transition states can be stabilized by the methyl group.

With the above mechanistic insights, here we report our understanding of why type-I instead of type-II cycloisomerization takes place for 1,6-enyne substrates shown in reactions 2 and 3 (Scheme 2). Also, we want to answer how and why the byproducts of type-III dienes are generated in reactions 2 and 3; therefore, we used DFT calculations to study model reactions *b* and *c* (Scheme 3) and to explore their possible pathways to type-I, II, and III dienes. Experimentally, Chatani did not study the 1,6-enyne substrates with substituents at both C1 and C4 positions. Here we report our experimental and DFT investigation of the cycloisomerization of this new substrate under the catalysis of $InCl_3$ (Our DFT investigation used model reaction *d* in Scheme 3. In the experimental investigations, we used substrates with a different tether, see Scheme 6 later for detail). Meanwhile, we tried to provide a unified model to explain how the type-I, II, and III dienes are generated and to understand how substituents affect the final reaction outcomes. The present investigation of mechanisms and factors affecting the regioselectivity in the cycloisomerization reaction will help chemists understand, predict, and develop new cycloisomerization reactions and new catalysts. This study will also prompt chemists to think more about the nature of other Lewis acids of IIIA metals in their reactions.

RESULTS AND DISCUSSION

1. Mechanism of Model Reaction *b*. *a. Type-I Diene Formation Pathway of the Model Reaction b.* DFT

Received: January 10, 2014
Published: March 25, 2014

   dx.doi.org/10.1021/jo500059j | *J. Org. Chem.* 2014, 79, 3809−3820

Scheme 1. 1,6-Enynes Cyloisomerizations

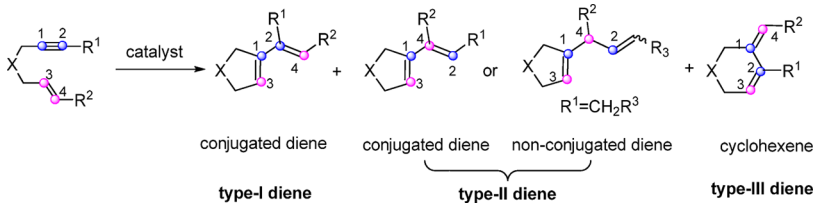

Scheme 2. Selected Examples of $InCl_3$-Catalyzed 1,6-Enyne Cycloisomerizations

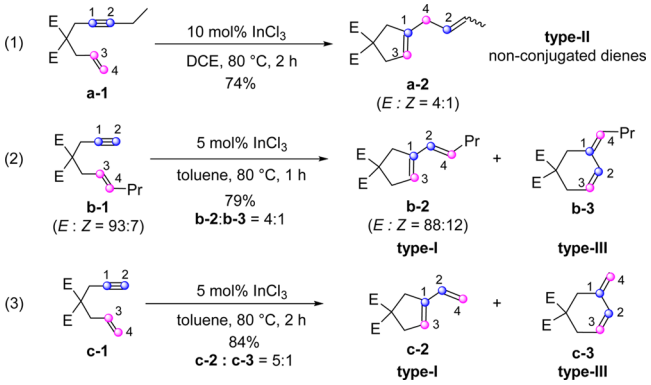

calculations indicate that $InCl_2^+$-catalyzed cycloisomerization of reaction *b* starts with catalyst transfer between 1,6-enyne **b-4** and the $InCl_2^+$/type-I product complex **b-11** (Figure 2). Meanwhile, a solvent molecule,[14] here a benzene molecule, is released, giving $InCl_2^+$/1,6-enyne complex **b-5**. Then the benzene molecule coordinates to the In atom of complex **b-5**, giving complex **b-6**. The In atom in complex **b-6** is coordinated by two chlorine atoms, an alkyne group, and a benzene molecule. The originally coordinated alkene moiety in **b-5** is released to become a spectator ligand in **b-6**. Then a nonclassical cyclopropanation process generates the cationic species of **b-7**, which can be regarded as a homoallylic cation or a nonclassical cyclopropane molecule. This can be appreciated from the structure of **b-7**, in which the C1−C2 bond is a double bond with a bond distance of 1.36 Å, the C1−C4 bond is a single bond with a bond distance of 1.63 Å, and the C1−C3 bond is partially formed with a bond distance of 1.85 Å.

Homoallylic cation **b-7** is then transformed to cyclobutyl cation **b-8** via **b-TS2**. This step can be understood by a two-step sequence: formation of a cyclopropyl carbinyl cation (CPC cation) first through the C1−C3 bond formation, followed by a [1,2]-C4 migration through the C1−C4 bond breakage and C2−C4 bond formation. Even though **b-8** can be regarded as a cyclobutyl carbocation with the positive charge mainly at the C1 atom, the C4 atom in it forms weak bonds with the C1, C2, and C3 atoms, as judged by the bond distances of d_{C4-C1} = 1.76 Å, d_{C4-C2} = 1.65 Å and d_{C4-C3} = 1.67 Å. It is noteworthy that in model reactions *c* and *d*, no such kind of cyclobutyl carbocations as **c-8** and **d-8** can be located computationally. This will be seen in what follows.

The following step is the C4−C3 bond breakage via transition state **b-TS3**, converting **b-8** to a more stable spiro cation **b-9**. This intermediate can also be viewed as a CPC cation with positive charge at the C3 atom if we think that C1 and C4 have a weak bond (d_{C1-C4} = 1.83 Å). This structure can also be understood as the interaction between the C4 cation and the C1═C3 bond.

The next step of the type-I diene formation pathway is the breakage of the weak C1−C4 bond and the coordination of the In atom by the C3═C4 bond, producing a type-I diene/$InCl_2^+$

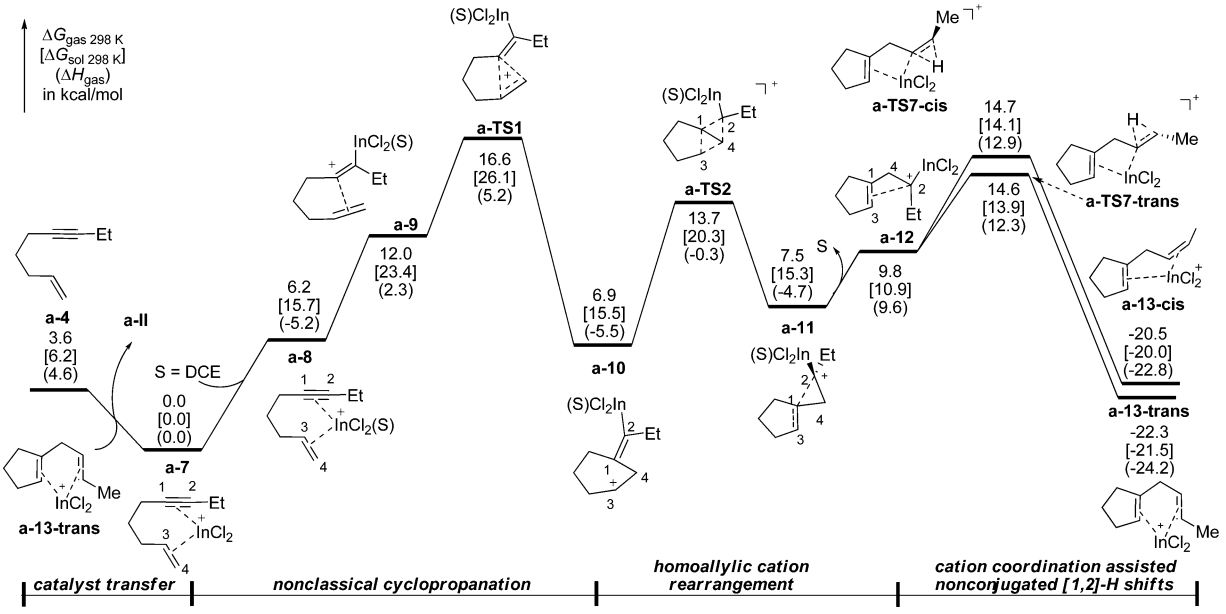

Figure 1. Previously reported density functional theory (DFT)-computed energy surface of $InCl_3$-catalyzed type-II cycloisomerization of 1,6-enyne (model reaction *a* in Scheme 3 of this paper).[12]

dx.doi.org/10.1021/jo500059j | J. Org. Chem. 2014, 79, 3809−3820

Scheme 3. Model 1,6-Enynes Cycloisomerization Reactions Used for Computational Studies

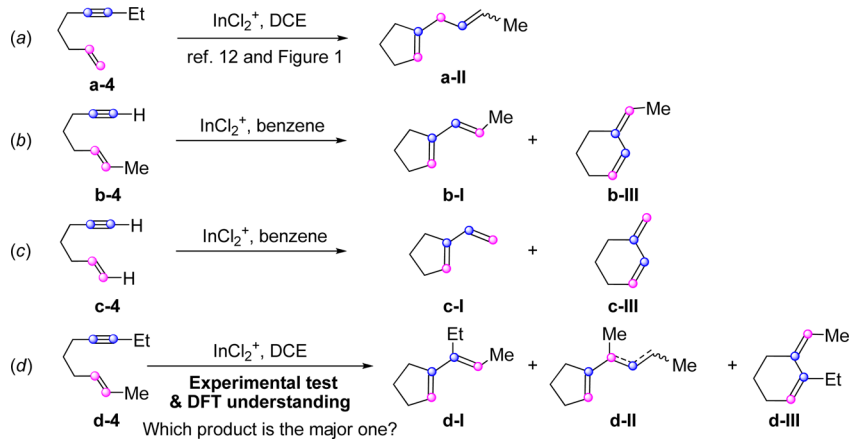

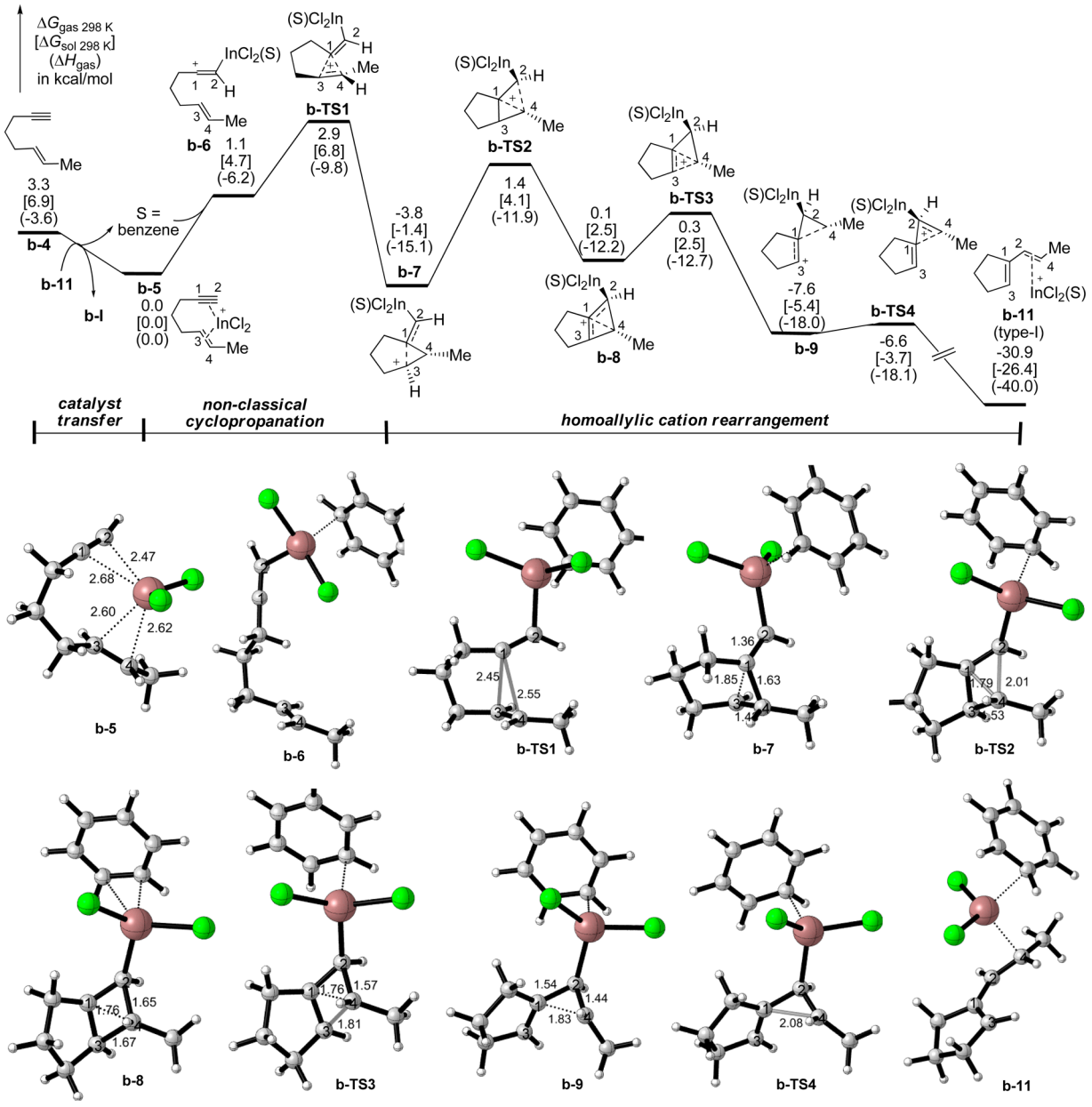

Figure 2. Energy surface and selected structures of the type-I diene formation pathway of the 1,6-enyne cycloisomerization reaction of **b-4** (reaction *b* in Scheme 3) in toluene solution (distances in Å).

dx.doi.org/10.1021/jo500059j | J. Org. Chem. 2014, 79, 3809−3820

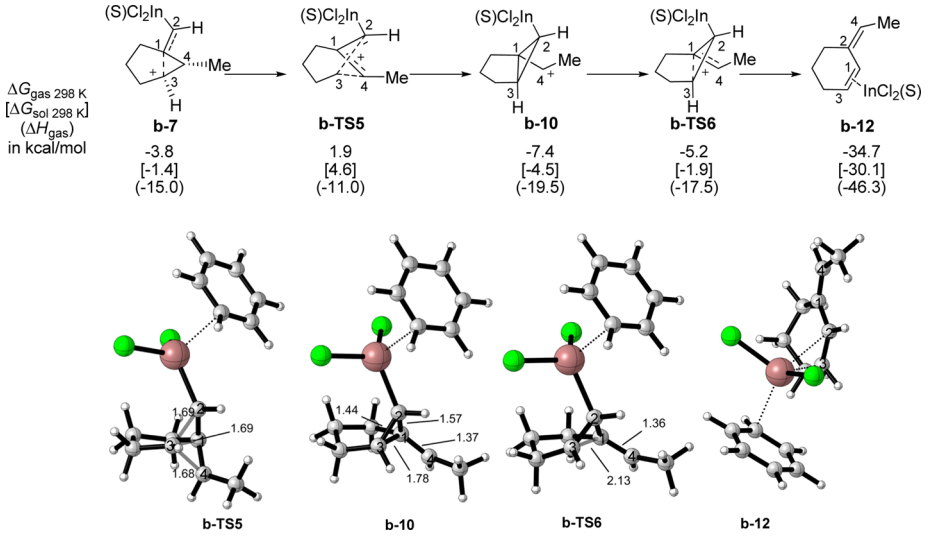

Figure 3. Energy surface and selected structures of the type-III diene formation pathway of the 1,6-enyne cycloisomerization reaction of **b-4** (reaction *b* in Scheme 3) in toluene solution (distances in Å).

Scheme 4. A Unified Model To Explain the Homoallylic Cation Rearrangements Leading to Different Products

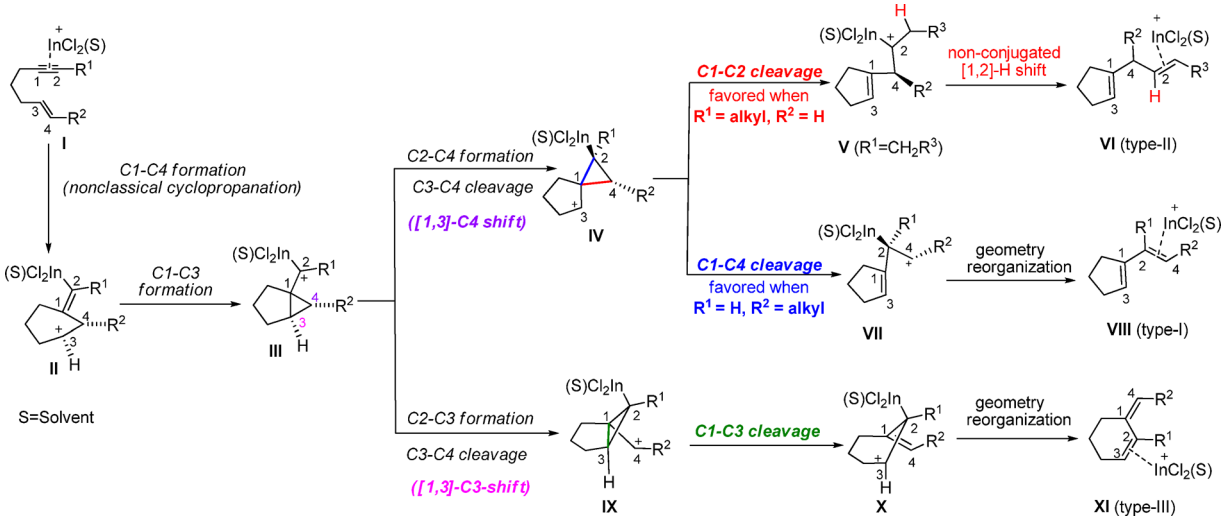

complex with an activation free energy of 1.0 kcal/mol. The corresponding transition state for this step is **b-TS4**, in which the C1−C4 bond is becoming elongated with respect to that in **b-9**. Intrinsic reaction coordinate (IRC) calculations suggested that **b-TS4** is connected by **b-9** and the type-I diene/$InCl_2^+$ complex, **b-11**.

In summary, the type-I cycloisomerization starts with nonclassical cyclopropanation, followed by homoallylic cation rearrangement, which includes CPC cation's [1,2]-rearrangement, formation of a cyclobutyl carbocation, generation of the CPC cation **b-9** via C3−C4 bond cleavage, and diene coordination. The most difficult step of the catalytic cycle is the homoallylic cation rearrangement from **b-7** to **b-TS2**, requiring an activation free energy of 5.2 kcal/mol. Experimentally, reaction 2 (Scheme 2) was carried out at 80 °C. We hypothesized that, even though the cycloisomerization by $InCl_2^+$ is easy, the generation of the catalytic species from $InCl_3$ could need a significant amount of activation energy to initiate the reaction for each catalytic cycle. Further discussion of the relationship of the catalyst generation and the catalytic cycle will be presented in section 6 of this part.

b. Type-III Diene Formation Pathway of the Model Reaction b. Experimentally, reaction 2 (Scheme 2) also produced the type-III diene product **b-3** as a byproduct. Our DFT calculations suggested that the generation of a type-III diene product was due to the existence of another competing rearrangement pathway from the homoallylic carbocation **b-7**. In the type-I diene formation pathway (Figure 3), **b-7** undergoes [1,2]-C4 migration with simultaneous C1−C3 and C2−C4 bond formations and C1−C4 bond cleavage via **b-TS2**, with an activation free energy of 5.2 kcal/mol. However, in the type-III diene formation pathway, **b-7** can simultaneously undergo the C2−C3 bond formation and C3−C4-bond breakage via **b-TS5**, generating CPC cation **b-10**, in which the positive charge can be regarded as residing at the C4 atom. Then the C1−C3 bond in **b-10** is completely cleaved via **b-TS6**, giving the final type-III diene/$InCl_2(S)^+$ complex, **b-12**.

From the above discussion, we can see that the bifurcation point for the two products (type-I vs type-III diene formation pathways) is complex **b-7**. Type-I diene formation pathway via **TS2** is slightly favored over the type-III diene formation pathway via **TS5** by 0.5 kcal/mol, suggesting that both type-I

dx.doi.org/10.1021/jo500059j | J. Org. Chem. 2014, 79, 3809−3820

Scheme 5. Selectivity Discussion of Type-I and Type-II Diene Formations[a]

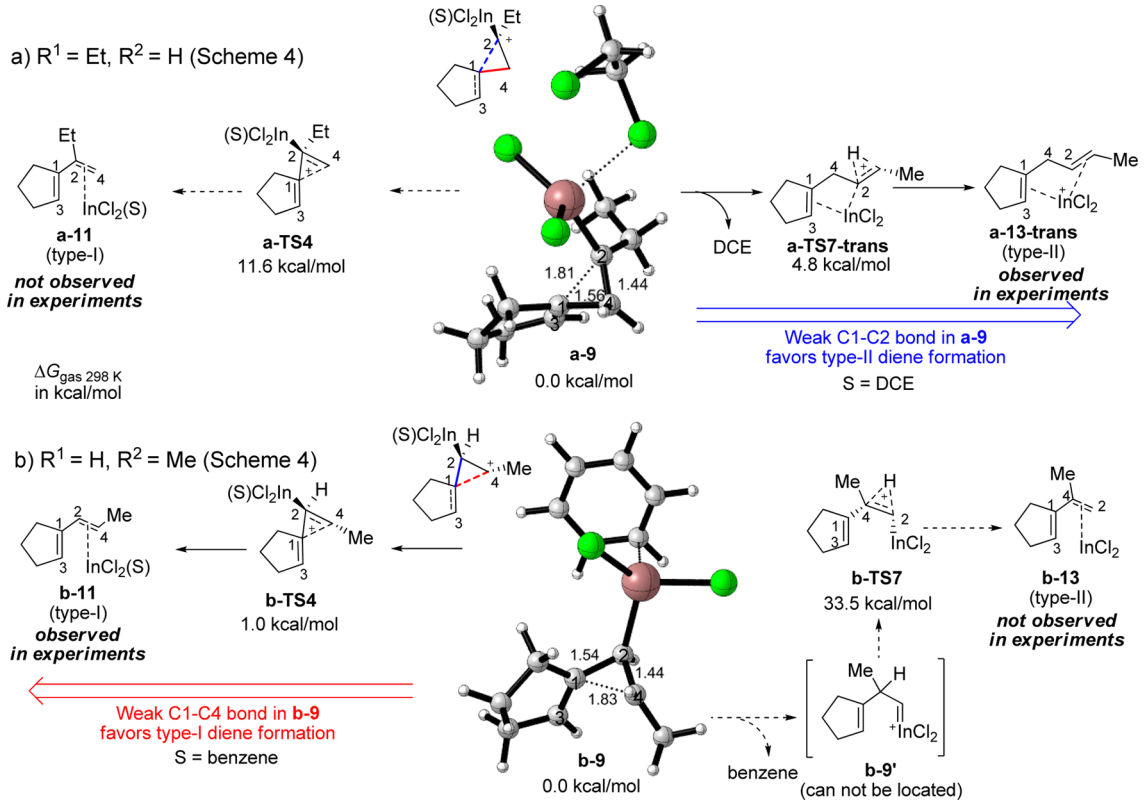

[a]The given energies are Gibbs free energy in the gas phase and distances are measured in Å.

diene and type-III diene can be generated, with the former as the major product. This is consistent with experimental observations, showing that the generation of a type-I diene product is slightly preferred over the generation of a type-III diene product (**b-2**:**b-3** = 4:1 in reaction 2 of Scheme 2).

2. A Unified Model To Explain the Chemoselectivity of $InCl_3$-Catalyzed Cycloisomerization of 1,6-Enynes. *a. Homoallylic Cation Rearrangements.*[15] On the basis of the discussed studies together with the previous results summarized in Figure 1, here we provide a unified model to explain how the homoallylic cation rearranges into different products via the type-I, II, and III diene formation pathways (Scheme 4). Similar type-I and type-II processes catalyzed by Au have been proposed and discussed by Echavarren and co-workers.[13c]

The cycloisomerization to different products is initiated by the $InCl_2^+$ activation of the triple bond of 1,6-enyne, generating a nonclassical homoallylic cation **II** via a C1−C4 bond formation from the $InCl_2^+$/1,6-enyne complex **I**. Then **II** is converted into CPC cation **III**, which is the bifurcation point for further type-I/II and type-III diene formation pathways. Two possible [1,3]-C shift transformations compete with each other via either a [1,3]-C4 shift to give intermediate **IV** (for type-I or type-II diene formation), or a [1,3]-C3 shift to give intermediate **IX** (for type-III diene formation).

Intermediate **IV** can then undergo the C1−C2 bond cleavage, giving intermediate **V**. A nonconjugated [1,2]-H shift converts **V** into the type-II diene product, **VI**. This can be called a double-bond cleavage[13c] pathway since both C1−C2 and C3−C4 bonds are broken in the final diene product. Intermediate **IV** can also undergo the C1−C4 bond cleavage, giving intermediate **VII**. Geometry reorganization then forms the diene−In complex **VIII**, which finally gives a type-I diene via dissociation of the In catalyst. This pathway can be viewed as a single-bond cleavage pathway[13c] since only the C3−C4 bond has been cut while the C1−C2 bond is intact in the final product. Intermediate **IX** (from **III**) can undergo the C1−C3 bond cleavage. This gives intermediate **X**, which can then give a type-III diene product through geometry reorganization.

From the above model, we can see that the key step determining the overall regiochemistry is the formation of **IV** or **IX**. The second key step is formation of either **V** or **VII** from **IV**. Different substituents can affect the energies of the corresponding transition states, and consequently, different products can be formed.

b. Why Type-I and III But Not Type-II Diene Formation? With the above model, we can now understand how the substituents in both the alkyne and alkene moieties of 1,6-enynes affect the selectivity of type-I and III dienes (Figure 2 and Figure 3) as well as type-II dienes (Figure 1). Scheme 4 gives some suggestions about the preference of one pathway over the other. If R^1 = alkyl and R^2 = H, the type-II diene formation pathway is favored because the alkyl group (R^1) can stabilize the generating cation at C2 in intermediate **V**. In this case, intermediates **VII** and **IX** with the cations located at C4 atoms cannot be accessed, and consequently, both type-I and type-III pathways cannot take place. This is supported by the computational results, showing that the [1,3]-C3 shift transition state (type-III pathway) starting with **a-10** (Figure 1) cannot be located. For the same reason, when R^1 = H and R^2 = alkyl, type-I and type-III diene formation pathways will be favored because the C4 cation in intermediate **VII** and **IX** can be stabilized by the R^2 group. Meanwhile, the [1,3]-C4 shift (type-I pathway)

dx.doi.org/10.1021/jo500059j | J. Org. Chem. 2014, 79, 3809−3820

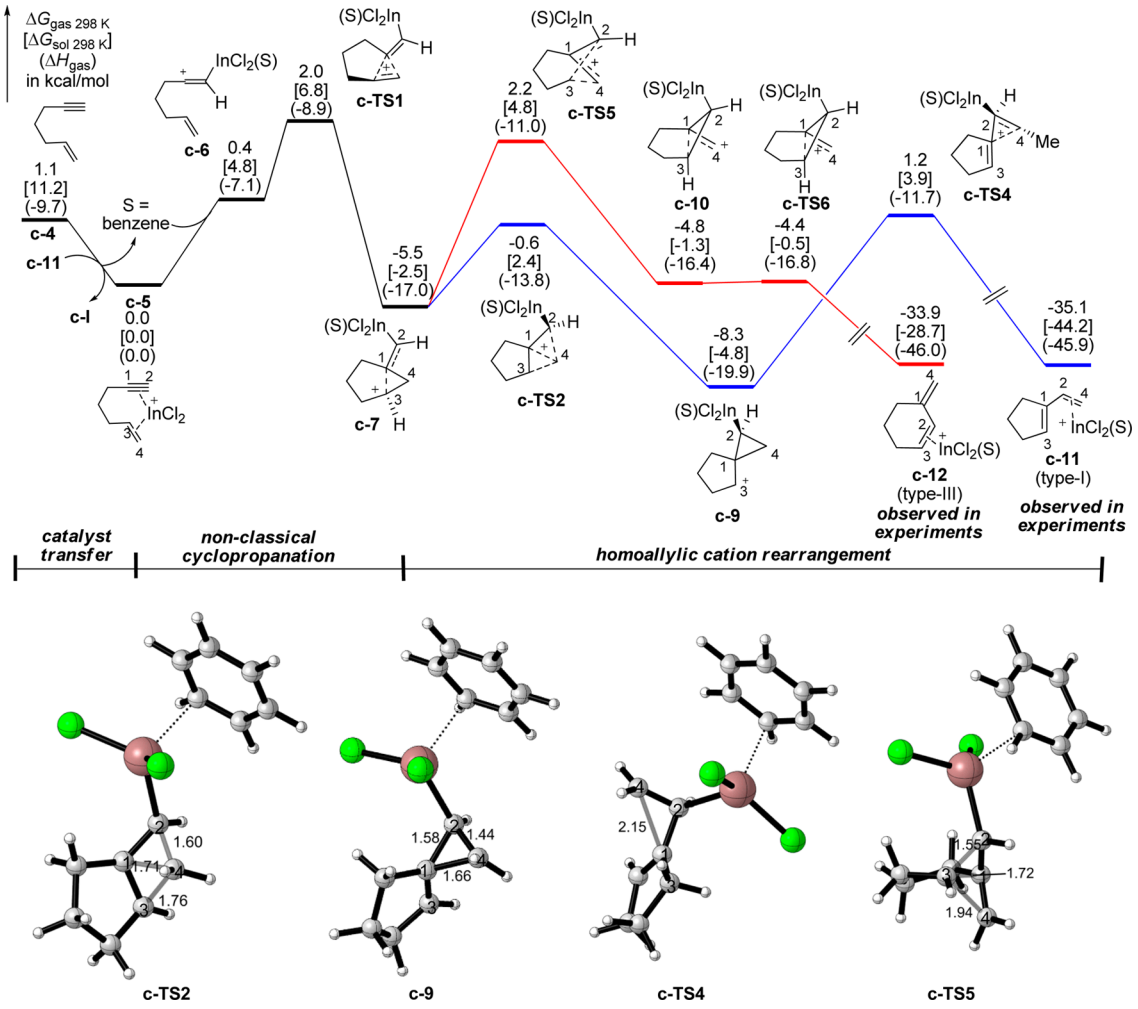

Figure 4. Energy surface and selected structures of the type-I diene formation of the 1,6-enyne cycloisomerization reaction of **c-4** (model reaction *c* in Scheme 3) in toluene solution (distances in Å).

and [1,3]-C3 shift (type-III pathway) have similar energy barriers; therefore, reaction 2 of Scheme 2 is more likely to give the type-I diene product together with the type-III diene product, while reaction 1 will only give type-II dienes. In what follows, we give more details about the selectivity between type-I and type-II diene formations.

Here we provide a comparison of the structures of **a-9** and **b-9**, which are key intermediates for giving type-II and type-I diene products, respectively (Scheme 5). In **a-9**, the corresponding R^2 = H suggests that **a-9** has the form of intermediate **V** instead of **VII**. This claim can be appreciated by the long C1−C2 bond (1.81 Å) and short C1−C4 bond (1.56 Å). Therefore, the positive charge in the cation is mainly located at the C2 atom, which favors a nonconjugated [1,2]-H shift reaction with an activation free energy of 4.8 kcal/mol. Breaking the C1−C4 bond in **a-9** and a subsequent [1,2]-H shift via **a-TS4** can give type-I diene product, but this requires an activation free energy of 11.6 kcal/mol, 6.8 kcal/mol higher than that of the type-II diene formation pathway. Consequently, reaction 1 in Scheme 2 gives a type-II diene product.

In **b-9**, the corresponding R^2 = Me, the positive charge in the cation is mainly located at the C4 atom. Consequently, the C1−C4 bond is very weak with a bond distance of 1.83 Å while the C1−C2 bond is strong with a bond distance of 1.54 Å. Because of this, reorganization of the coordination around $InCl_2^+$ is easy, giving a type-I diene product. If **b-9** adopts the type-II diene formation pathway, it has to break the strong C1−C2 bond and this is energetically difficult (we found that the corresponding **b-9′** is not a minimum and cannot be located computationally). Additional evidence to exclude the type-II diene formation pathway is that, supposing that **b-9′** can be generated, its later [1,2]-H shift is very difficult, with a computed activation free energy of 33.5 kcal/mol.

3. Mechanism of Model Reaction *c*. When R^1 = H and R^2 = H, we also found that both type-I and type-II diene formation pathways are favored. Calculations suggested that **c-4** (corresponding to reaction 3 in Scheme 2) can take both type-I and type-III diene formation pathways and the computed energy surface is summarized in Figure 4. The type-I diene formation pathway is still favored over the type-III diene formation pathway by 1.0 kcal/mol (**c-TS4** vs **c-TS5**), suggesting that a type-I diene as the major product and a type-III diene as the minor product are generated. These calculation results agree with the experimental observation (reaction 3 in Scheme 2) where a mixture of type-I and type-III dienes with a ratio of 5:1 was generated.

A close look at intermediate **c-9** uncovers the reasons why the type-II diene pathway is disfavored. Because of corresponding R^1 = H and R^2 =H, no functional group can stabilize the cation on the C2 or C4 atom in **c-9**. Consequently, the cation is

dx.doi.org/10.1021/jo500059j | J. Org. Chem. 2014, 79, 3809−3820

Scheme 6. New Experimental Results of $InCl_3$-Catalyzed 1,6-Enyne Isomerization of Enynes with Substituents at Both the Alkyne and Alkene Parts

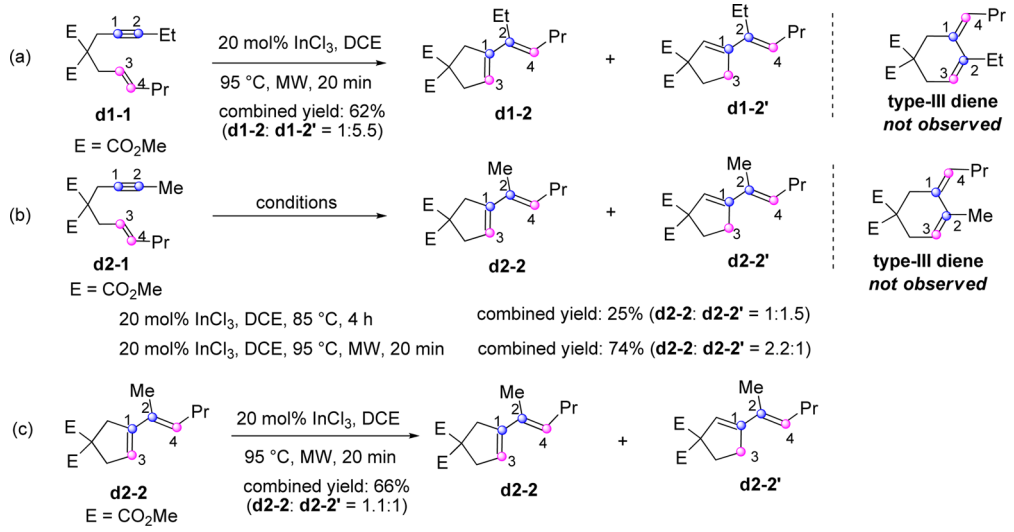

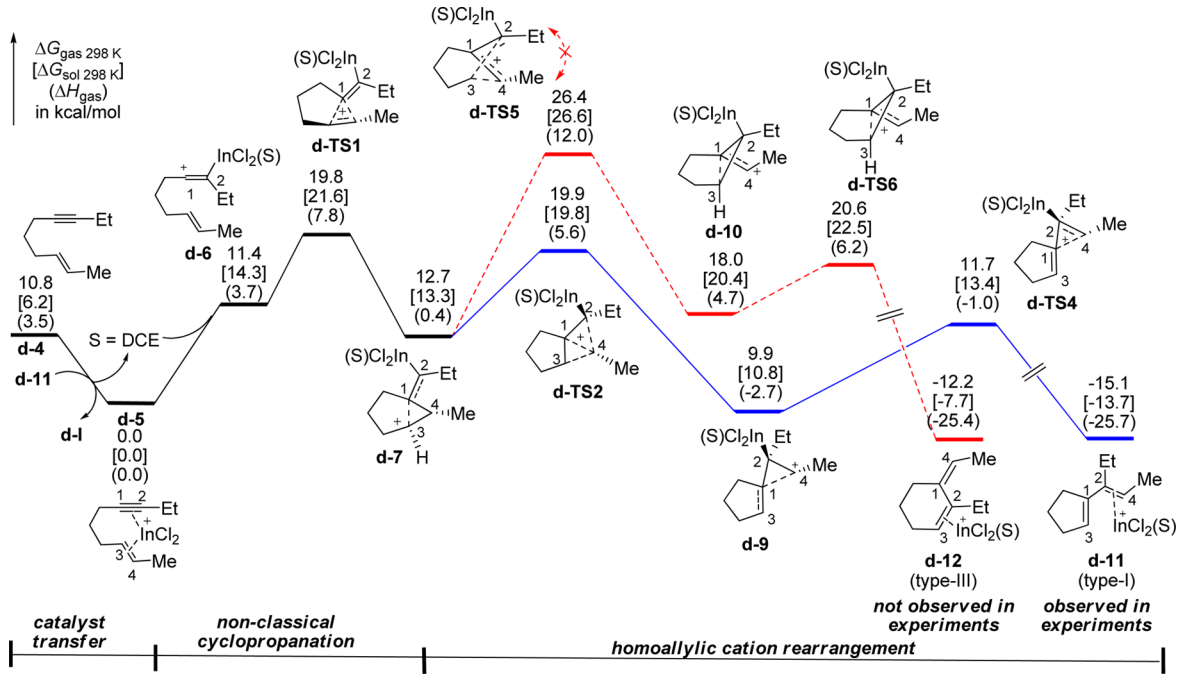

Figure 5. Energy surface of the type-I 1,6-enyne cycloisomerization reaction of **d-4** in 1,2-dichloroethane (DCE) solution (model reaction *d* in Scheme 3).

best distributed to the whole system. In this case, C1−C2 and C1−C4 bonds become stronger, as indicated by their bond distances (d_{C1-C2} = 1.58 Å and d_{C1-C4} = 1.66 Å); therefore, breaking the C1−C4 bond and geometry reorganization are easier and will give a type-I diene product with an activation free energy of 9.5 kcal/mol.

4. Cycloisomerization of 1,6-Enyne with R^1 = Alkyl, R^2 = Alkyl (Model Reaction *d*): Experiments and Calculations. *a. Experimental Results.* In previous reports from Chatani's group,[4] there was no experimental study of how 1,6-enyne substrates with alkyl groups at both the C1 and C4 atoms reacted using a $InCl_3$ catalyst. Therefore, we carried out a new experimental study of the cycloisomerization of **d1-1** and **d2-1**, showing that in these cases, only type-I dienes were generated under microwave (MW) irradiation at 95 °C (Scheme 6). Here, the type-I dienes are mixed with their corresponding olefin isomerization products (**d1-2′** and **d2-2′**). Further experimentation in Scheme 6c indicated that **d2-2′** was generated by double bond isomerization of the type-I product **d2-2**. Here we point out that the reaction in Scheme 6b could also take place in an oil bath at 85 °C in 4 h, giving 25% yield of **d2-2** and **d2-2′** together with other unknown products. We carried out this reaction at a higher temperature (95 °C) under MW irradiation for a shorter time (20 min), giving a better yield of the dienes (74%). It is interesting to find that the yields of cycloisomerizations and the ratio of the two products under MW irradiation varied (see the experimental part) and that the reason for this is not yet known.

b. Computed Reaction Energy Surface. Figure 5 presents the computed energy surface for the cycloisomerization of **d-4**

dx.doi.org/10.1021/jo500059j | J. Org. Chem. 2014, 79, 3809−3820

Scheme 7. Selectivity Discussion of Type-I and Type-II Diene Formations[a]

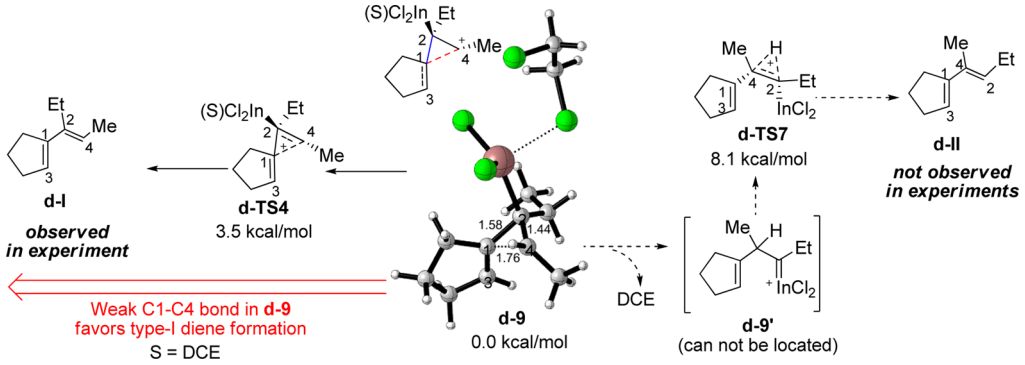

[a]The given energies are Gibbs free energy in the gas phase and bond distances are measured in Å.

to give both type-I diene and type-III diene products. One significant difference for the present reaction of **d-4** compared to the previous ones (**b-4** and **c-4**) is that the present reaction requires a much higher cyclopropanation energy barrier: 8.4 kcal/mol for **d-6** to **d-TS1**, while 1.8 kcal/mol is required for **b-6** to **b-TS1** and 1.6 kcal/mol is required for **c-6** to **c-TS1**. This is because the generation of **b-6** and **c-6** from **b-5** and **c-5** are both exothermic, while the generation of **d-6** from **d-5** is endothermic by 3.7 kcal/mol. We attribute this difference to the stronger binding of **d-4** than that of **b-4** and **c-4** to $InCl_2^+$ due to the presence of an additional ethyl group in **d-4**.

c. Type-I Diene Formation Pathway vs Type-II Diene Formation Pathway. Calculations indicated that once the CPC cation **d-9** is formed, it can easily undergo the C1−C4 bond cleavage via transition state **d-TS4**. This requires an activation free energy of 3.5 kcal/mol. The competing type-II diene formation pathway involves breaking the C1−C2 bond and a [1,2]-H shift process. We found that the corresponding intermediate from the C1−C2 bond cleavage cannot be located, and the subsequent [1,2]-H shift transition state **d-TS7** was disfavored by 4.6 kcal/mol than **d-TS4** (Scheme 7). We attribute these phenomena to the weak C1−C4 bond in CPC cation **d-9**. The bond length of the C1−C4 bond in **d-9** is 1.76 Å, while the bond length of the C1−C2 bond is 1.58 Å. Thus, the C1−C4 bond cleavage transition state **d-TS4** is favored by 4.6 kcal/mol over the [1,2]-H shift transition state **d-TS7**, suggesting that type-I diene products should be generated. This DFT prediction is consistent with the experimental results shown in Scheme 6.

d. Type-I Diene Formation Pathway vs Type-III Diene Formation Pathway. Cyclopropane intermediate **d-7** can undergo either the [1,3]-C3 shift via **d-TS5** to give a type-III diene product, or the [1,2]-C4 shift via **d-TS2** to produce a type-I diene product. DFT calculations found that **d-TS2** is more favored than **d-TS5** by 6.5 kcal/mol, which is consistent with our experimental observation that only type-I diene products were obtained. In **d-TS5** corresponding to the formation of the C2−C3 bond (Figure 6), Et (on C2) and Me (on C4) groups displayed a 1,3-eclipsing interaction, as judged by the small C5−C2−C4−C6 dihedral angle (−0.65°) and the short H1−H2 distance (1.92 Å). This repulsion increases the activation energy of the [1,3]-C3-shift process from 5.7 kcal/mol (**b-TS5** in Figure 3) to 11.6 kcal/mol (**d-TS5** in Figure 5). Consequently, when both of the terminal positions of alkene and alkyne (C2 and C4) were substituted by the alkyl groups, only the type-I diene products were observed

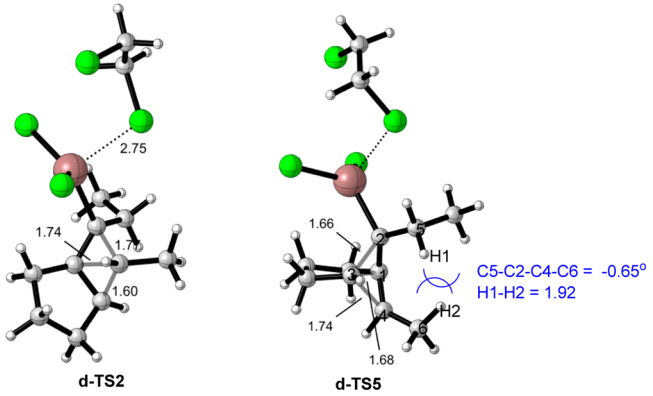

Figure 6. Structures of **d-TS2** and **d-TS5** (distances in Å).

and the type-III diene formation pathway was suppressed due to the steric repulsion between R^1 and R^2 groups.

5. Further Computational Results Suggesting That $InCl_3$ Is Not the Catalytic Species. The above computational results using $InCl_2^+$ as the real catalytic species agree with the experimentally observed regiochemistry. Here we further support that $InCl_3$ is not the real catalyst (Table 1). In the cases of using $InCl_3$ as the possible catalytic species, calculations predicted that the type-I diene formation pathways were favored by 2.5 and 3.7 kcal/mol over the type-III diene formation pathways for both reactions *b* and *c*, suggesting that type-III dienes should not be obtained. This is in contrast to the experiments, because reactions 2 and 3 of Scheme 2

Table 1. Comparison of the Regioselectivities between the Experimental and Computational Results Using $InCl_2^+$ and $InCl_3$ as the Catalytic Species

		DFT computed $\Delta\Delta G^{a,b}$	
model reaction	ratio of type-I diene/type-III diene (experimental result)	$InCl_3$ as the catalytic species	$InCl_2^+$ as the catalytic species
b	4:1 (Scheme 2)	−2.5 (35:1)	−0.5 (2:1)
c	5:1 (Scheme 2)	−3.7 (>99:1)	−1.0 (4:1)
d	1:0 (Scheme 6)	−10.2 (>99:1)	−6.6 (>99:1)

[a]$\Delta\Delta G$ is the Gibbs energy difference (computed in the gas phase) between the regio-determining transition states leading to type-I dienes and type-III dienes ($\Delta\Delta G = \Delta G_{\text{type-I}} - \Delta G_{\text{type-III}}$). Energy in kcal/mol. [b]The number in parentheses is the DFT predicted ratio of type-I diene to type-III diene at corresponding temperature.

dx.doi.org/10.1021/jo500059j | J. Org. Chem. 2014, 79, 3809−3820

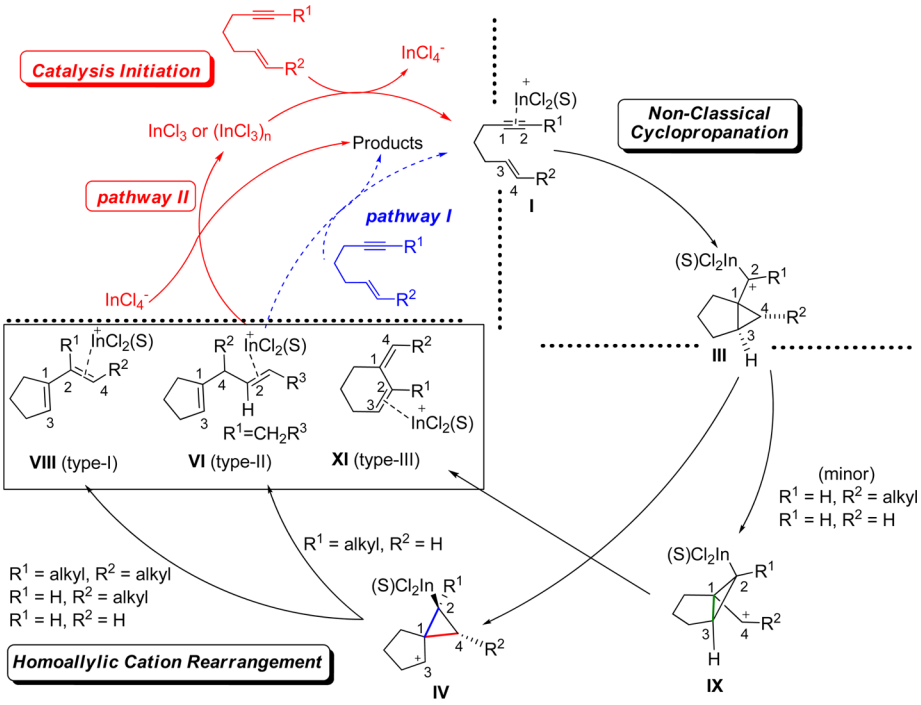

Figure 7. Catalytic cycle of $InCl_3$-catalyzed cycloisomerizations of 1,6-enynes.

produced mixtures of type-I and type-III dienes with a ratio of 4:1 and 5:1, respectively. Only for reaction *d*, did DFT calculations using $InCl_3$ as the possible catalytic species give the same selectivity as that which was observed by our experiment. Previously we have shown that $(InCl_3)_2$ is not the real catalytic species because calculations using $(InCl_3)_2$ as the catalytic species gave the similar selectivity as calculations using $InCl_3$ as the catalytic species. Therefore, we ruled out this possibility of $(InCl_3)_2$ as the real catalyst and did not do further DFT calculations in the reactions *b*–*d*.

6. Further Discussion of the Catalyst Transfer Step and the Reaction Activation Energy. The above calculations using model reactions *a*–*d* (Scheme 3) gave an in-depth understanding of the catalytic cycles. Calculations showed that all of these catalytic cycles should be easy because the activation barriers are very low (16.6, 5.2, 9.5, and 19.9 kcal/mol for model reactions *a*, *b*, *c*, and *d*, respectively). In contrast, all of these reactions had to be carried out at high temperature: 80 °C for reactions 2 and 3 in Scheme 2, and 95 °C under MW radiation or a heated oil bath at 85 °C for reactions in Scheme 6. Therefore, we hypothesized that once a catalytic cycle is finished, there is no catalyst transfer step from the product–catalyst complex to the substrate–catalyst (pathway I in Figure 7). Instead, the catalytic species $InCl_2^+$ could quickly associate with $InCl_4^-$ to form $InCl_3$ (or its dimer) again (pathway II in Figure 7); therefore, each catalytic cycle requires generation of the catalytic species. This could be the most energy demanding, and consequently, the cycloisomerization of all 1,6-enynes catalyzed by $InCl_3$ requires a temperature of 80 °C or higher. More studies are required to understand whether or not these hypotheses are correct.

■ CONCLUSION

Through DFT calculations on model reactions *a*–*d* (Scheme 3), we obtained a unified model to explain how the type-I, type-II, and type-III diene products are generated in $InCl_3$-catalyzed cycloisomerizations of 1,6-enynes with different substituents (Scheme 4 and Figure 7). DFT calculations further supported that the catalytic species is $InCl_2^+$, but not $InCl_3$. DFT calculations indicated that the entire catalytic cycle of the cycloisomerization starts with a nonclassical cyclopropanation of the vinyl cation (formed by coordination of $InCl_2^+$ to the alkyne) to the alkene moiety, giving a homoallylic cation **III**. This homoallylic cation can undergo different rearrangements depending on the substituents on the terminal positions of alkene (R^2) and alkyne (R^1) of the substrates. One rearrangement involves the C3–C4 bond cleavage and C2–C4 bond formation, yielding intermediate **IV**. If R^2 = alkyl group, **IV** undergoes direct geometry reorganization to give a conjugated type-I diene. In this case, the type-I diene formation pathway has a competitive rearrangement reaction of intermediate **III**, which directly undergoes the C3–C4 bond cleavage but without C2–C4 bond formation. This rearrangement gives a type-III diene product, cyclohexene, and is only slightly disfavored compared to the formation of a conjugated diene. However, if R^1 = ethyl and R^2 = H, the C1–C4 bond cleavage from intermediate **IV** will not be favored because this process generates a less stable carbocation at the C4 atom. Instead, intermediate **III** undergoes a C1–C2 bond cleavage, followed by a $InCl_2^+$ coordination assisted nonconjugated [1,2]-H shift to give nonconjugated type-II dienes. DFT calculations and experiments found that, if R^1 = alkyl and R^2 = alkyl, only the type-I dienes would be generated because the type-III diene formation pathway suffers a steric repulsion between R^1 and R^2 in the C1–C3 bond formation transition state (Figure 6).

■ COMPUTATIONAL METHODS

All calculations were performed with the Gaussian 09 program.[16] All gas phase stationary points were optimized using the 3-parameter hybrid Becke exchange/Lee–Yang–Parr correlation functional (B3LYP).[17] The LANL2DZ pseudo-potential and basis set[18] were used for the In atom, and the 6-31G(d) basis set[19] was used for the other atoms (keyword 5D was used in the calculations). Full Hessian

dx.doi.org/10.1021/jo500059j | J. Org. Chem. 2014, 79, 3809–3820

matrices in Gaussian 09 were calculated to verify the nature of all of the stationary points as either minima or first-order saddle points. The first-order saddle points were further characterized by IRC[20] calculations to confirm that the stationary points were correctly connected to the corresponding reactants and products. Solvation corrections to free energies were performed using universal force field (UFF) radii and a dielectric conductor-like polarizable continuum model (CPCM)[21] in toluene or DCE (these two solvents were used in the experiments). Solvation calculations were carried out on the gas-phase optimized structures. All of the energies discussed in the paper and the Supporting Information are Gibbs free energies in the gas phase at 298 K ($\Delta G_{\text{gas 298K}}$). Gibbs energies at 298 K in solution ($\Delta G_{\text{sol 298K}}$) (here the entropies were approximated by using the gas-phase computed entropies) and gas phase enthalpies (ΔH_{gas}) are also provided for reference. We found that the B3LYP method can reproduce the experimentally observed regioselectivity while calculations using B3LYP-D, M06, and M06-2X functionals could not. This suggests that B3LYP is a good choice for investigating the present cationic In-catalyzed cycloisomerizations of 1,6-enynes (for more discussion, see the Supporting Information).

EXPERIMENTAL SECTION

All NMR spectra were recorded on a 400 MHz spectrometer, except for **d1-2** which was recorded on a 500 MHz spectrometer. ^{1}H and ^{13}C NMR spectra were recorded using the deuterated solvent as the lock and the residual solvent as the internal reference. High-resolution mass spectrometry (HRMS) was performed under an electrospray ionization (ESI) technique using a Fourier transform ion cyclotron resonance (FT-ICR) analyzer. Herein, we report our experimental results shown in Scheme 6.

(*E*)-Dimethyl 2-(Hex-2-enyl)-2-(pent-2-ynyl)malonate (d1-1). To a suspension of NaH (0.16 g, 6.6 mmol, washed with hexane) in 10 mL of tetrahydrofuran (THF), (E)-dimethyl 2-(hex-2-enyl)malonate (1.18 g, 5.5 mmol) was added dropwise at 0 °C over a period of 15 min. Then the mixture was stirred at room temperature (rt) until the evolution of hydrogen gas subsided. The mixture was cooled to 0 °C, and a solution of 1-bromopent-2-yne (0.88 g, 6.0 mmol) was added dropwise over a period of 15 min. After stirring for an additional 12 h at rt, water was added slowly at 0 °C, and the organic layer was separated. The aqueous layer was extracted with Et_2O, and the combined organic layers were washed with brine, dried over Na_2SO_4, and concentrated in vacuum. The residue was purified by column chromatography on silica gel (eluted with polyethylene/ethyl acetate (PE/EA) 30:1) to give **d1-1** as a colorless oil (1.22 g, 83% yield). ^{1}H NMR (400 MHz, $CDCl_3$, δ): 5.61−5.50 (m, 1H), 5.22 (dt, J = 15.0, 7.4 Hz, 1H), 3.72 (s, 6H), 2.73−2.71 (m, 4H), 2.16−2.12 (m, 2H), 1.98−1.93 (q, J = 7.0 Hz, 2H), 1.38−1.32 (m, 2H), 1.09 (t, J = 7.5 Hz, 3H), 0.87 (t, J = 7.3 Hz, 3H). ^{13}C NMR (101 MHz, $CDCl_3$, δ): 170.7, 135.8, 123.2, 84.9, 73.8, 57.6, 52.5, 35.4, 34.7, 22.9, 22.5, 14.2, 13.6, 12.4. FT-IR (neat) ν_{max} (cm^{-1}): 2961, 1743, 1441, 1289, 1207, 1058, 976. HRMS (ESI) (m/z): [M + H$^+$] calcd for $C_{16}H_{25}O_4$, 281.17474; found, 281.17457.

(*E*)-Dimethyl 2-(But-2-ynyl)-2-(hex-2-enyl)malonate (d2-1). Using the general procedure for synthesis of **d1-1**, **d2-1** (0.94 g, 71% yield) was obtained as a colorless oil from (E)-dimethyl 2-(hex-2-enyl)malonate (1.18 g, 5.5 mmol) and 1-bromobut-2-yne (0.79 g, 6.0 mmol). ^{1}H NMR (400 MHz, $CDCl_3$, δ): 5.61−5.50 (m, 1H), 5.22 (dt, J = 15.1, 7.5 Hz, 1H), 3.72 (s, 6H), 2.73−2.71 (m, 4H), 1.98−1.95 (m, 2H), 1.76 (t, J = 2.5 Hz, 3H), 1.41−1.29 (m, 2H), 0.87 (t, J = 7.4 Hz, 3H). ^{13}C NMR (101 MHz, $CDCl_3$, δ): 170.7, 135.8, 123.2, 78.7, 73.4, 57.5, 52.5, 35.40, 34.7, 22.9, 22.5, 13.5, 3.5. FT-IR (neat) ν_{max} (cm^{-1}): 2977, 1744, 1210, 990. HRMS (ESI) (m/z): [M + H$^+$] calcd for $C_{15}H_{23}O_4$, 267.15909; found, 267.15898.

General Procedure for the $InCl_3$-Catalyzed 1,6-Enyne Cycloisomerizations of d1-1 and d1-2 in DCE under MW Heating (Scheme 6). To a mixture of anhydrous DCE (2.5 mL) and $InCl_3$ (17.6 mg, 0.08 mmol) under argon, 1,6-enyne (**d1-1**, 0.4 mmol, 112 mg; or **d2-1**, 0.4 mmol, 106 mg) was added. The resulting mixture was stirred at 95 °C under MW heating for an additional 20 min. The reaction was cooled to rt and the reaction mixture was directly concentrated in a vacuum. The residue was subjected to flash column chromatography on silica gel (eluted with PE/EA 30:1 to 20:1) to give an inseparable mixture of diene products. The ratios of diene products were determined by ^{1}H NMR. The combined reaction yield of **d1-2** and **d1-2′** (as colorless oil with a ratio of 1:5.5, Scheme 6a) from **d1-1** was 62% (69 mg). The combined reaction yield of **d2-2** and **d2-2′** (as colorless oil with a ratio of 2.2:1, Scheme 6b) from **d2-1** was 74% (78 mg).

It is noteworthy that the yields of the cycloisomerizations and the ratio of the two products under MW irradiation varied and the reason for this is not known. These results are given here: for the reaction of **d1-1**, we also found the yield (ratio of **d1-2**:**d1-2′**) as 67% (1.4:1) and 71% (1.9:1); and for the reaction of **d2-1**, we also found the yield (ratio of **d2-2**:**d2-2′**) to be 74% (11:1), 72% (8.5:1), 54% (2.9:1), and 53% (2.3:1).

Procedure for the $InCl_3$-Catalyzed Isomerization of d2-2 to d2-2′ in DCE Under MW Heating (Scheme 6c). To a mixture of anhydrous DCE (2.5 mL) and $InCl_3$ (8.8 mg, 0.04 mmol) under argon, **d2-2** (0.2 mmol, 53 mg) was added. The resulting mixture was stirred at 95 °C under MW heating for an additional 20 min. The reaction was cooled to rt, and the reaction mixture was directly concentrated in a vacuum. The residue was subjected to flash column chromatography on silica gel (eluted with PE/EA 30:1 to 20:1) to give an inseparable mixture of dienes with **d2-2**:**d2-2′** = 1.1:1 (determined by ^{1}H NMR). The combined reaction yield of **d2-2** and **d2-2′** was 66% (35 mg).

General Procedure for the Au-Catalyzed 1,6-Enyne Cycloisomerizations. In the $InCl_3$-catalyzed reactions in Scheme 6, the type-I diene products and their olefin isomers were inseparable. To obtain pure type-I diene products and their NMR, the Au-catalyzed cycloisomerization reaction procedure[4d] was used as follows. Under Ar, a mixture of anhydrous DCE (2.5 mL), $AuPPh_3Cl$ (8.1 mg, 0.016 mmol), and $AgSbF_6$ (5.5 mg, 0.016 mmol) were stirred at rt for 20 min. Then the 1,6-enyne (**d1-1**, 0.4 mmol, 112 mg; or **d2-1**, 0.4 mmol, 106 mg) was added to the solution containing the gold catalyst. The resulting mixture was stirred at rt for an additional 20 min. The reaction mixture was then directly concentrated in a vacuum. The residue was subjected to flash column chromatography on silica gel (eluted with PE/EA 60:1) to give a pure type-I diene product (**d1-2** or **d2-2**). The yield of **d1-2** (from **d1-1**) was 89% (97 mg), as colorless oil. The yield of **d2-2** (from **d2-1**) was 78% (83 mg), as colorless oil. On the basis of the NMR data of the pure type-I diene products (**d1-2** and **d2-2**), the NMR spectra of olefin isomerization isomers (**d1-2′** and **d2-2′**) were resolved from the NMR spectra of the mixture of dienes.

(*E*)-Dimethyl 3-(Hept-3-en-3-yl)cyclopent-3-ene-1,1-dicarboxylate (d1-2). Obtained by Au-catalyzed cycloisomerization. ^{1}H NMR (500 MHz, $CDCl_3$, δ): 5.50 (s, 1H), 5.37 (t, J = 7.2 Hz, 1H), 3.74 (s, 6H), 3.15 (d, J = 1.4 Hz, 2H), 3.12 (s, 2H), 2.27−2.21 (m, 2H), 2.11−2.06 (m, 2H), 1.47−1.35 (m, 2H), 0.99 (t, J = 7.6 Hz, 3H), 0.92 (t, J = 7.4 Hz, 3H). ^{13}C NMR (126 MHz, $CDCl_3$, δ): 172.7, 140.9, 137.0, 128.6, 120.3, 58.5, 52.8, 41.0, 40.9, 30.0, 22.9, 21.5, 14.02, 13.95. FT-IR (neat) ν_{max} (cm^{-1}): 2977, 1741, 1439. HRMS (ESI) (m/z): [M + H$^+$] calcd for $C_{16}H_{25}O_4$, 281.17474; found, 281.17465.

(*E*)-Dimethyl 3-(Hept-3-en-3-yl)cyclopent-2-ene-1,1-dicarboxylate (d1-2′). ^{1}H NMR (400 MHz, $CDCl_3$, δ): 5.71 (s, 1H), 5.49 (t, J = 7.3 Hz, 1H), 3.73 (s, 6H), 2.64−2.55 (m, 2H), 2.50−2.47 (m, 2H), 2.35−2.25 (m, 2H), 2.13−2.07 (m, 2H), 1.44−1.38 (m, 2H), 1.02 (t, J = 7.5 Hz, 3H), 0.92 (t, J = 7.4 Hz, 3H).^{13}C NMR (101 MHz, $CDCl_3$, δ): 172.0, 148.2, 137.1, 130.7, 121.1, 66.5, 52.6, 31.8, 31.4, 30.1, 22.8, 21.6, 14.02, 13.96. Mixture of **d1-2** and **d1-2′**, FT-IR (neat) ν_{max} (cm^{-1}): 2969, 1736, 1438, 1251, 1076. Mixture of **d1-2** and **d1-2′**, HRMS (ESI) (m/z): [M + H$^+$] calcd for $C_{16}H_{25}O_4$, 281.17474; found, 281.17466.

(*E*)-Dimethyl 3-(Hex-2-en-2-yl)cyclopent-3-ene-1,1-dicarboxylate (d2-2). Obtained by Au-catalyzed cycloisomerization. ^{1}H NMR (400 MHz, $CDCl_3$, δ): 5.49 (s, 1H), 5.44 (t, J = 7.2 Hz, 1H), 3.74 (s, 6H), 3.17 (s, 2H), 3.10 (s, 2H), 2.12−2.08 (m, 2H), 1.78 (s, 3H), 1.46−1.34 (m, 2H), 0.91 (t, J = 7.4 Hz, 4H). ^{13}C NMR (101 MHz, $CDCl_3$, δ): 172.7, 142.6, 130.6, 129.1, 120.8, 58.7, 52.8, 41.0,

dx.doi.org/10.1021/jo500059j | J. Org. Chem. 2014, 79, 3809−3820

40.7, 30.4, 22.8, 13.9.[22] FT-IR (neat) ν_{max} (cm^{-1}): 2961, 1736, 1438, 1270, 1070. HRMS (ESI) (m/z): [M + H^+] calcd for $C_{15}H_{23}O_4$, 267.15909; found, 267.15890.

(*E*)-Dimethyl 3-(Hex-2-en-2-yl)cyclopent-2-ene-1,1-dicarboxylate (d2-2′). ^{1}H NMR (400 MHz, $CDCl_3$, δ): 5.69 (s, 1H), 5.55 (t, J = 7.1 Hz, 1H), 3.74 (s, 6H), 2.63 (t, J = 6.8 Hz, 2H), 2.54−2.44 (m, 2H), 2.14−2.07 (m, 2H), 1.83 (s, 3H), 1.46−1.36 (m, 2H), 0.91 (t, J = 7.2 Hz, 3H). ^{13}C NMR (101 MHz, $CDCl_3$, δ): 172.7, 145.0, 131.3, 130.7, 129.1, 66.5, 52.7, 31.6, 31.5, 30.4, 22.7, 14.0. Mixture of **d2-2** and **d2-2′**, FT-IR (neat) ν_{max} (cm^{-1}): 2961, 1736, 1441, 1263, 1069. Mixture of **d2-2** and **d2-2′**, HRMS (ESI) (m/z): [M + H^+] calcd for $C_{15}H_{23}O_4$, 267.15909; found, 267.15890.

■ ASSOCIATED CONTENT

Supporting Information

^{1}H and ^{13}C NMR spectra, computed thermodynamic data, and Cartesian coordinates of computed structures. This material is available free of charge via the Internet at http://pubs.acs.org.

■ AUTHOR INFORMATION

Corresponding Author

*E-mail: yuzx@pku.edu.cn.

Notes

The authors declare no competing financial interest.

■ ACKNOWLEDGMENTS

We are grateful for the generous financial support from the Natural Science Foundation of China (21232001) and the National Basic Research Program of China-973 Program (2011CB808600). We also thank Mr. Chi Zhang for repeating the experiments and Mr. Yang Gao and Dr. Wei Meng for checking the calculation results.

■ REFERENCES

(1) For recent reviews on the cycloisomerizations of 1, *n*-enynes, see: (a) Lee, S. I.; Chatani, N. *Chem. Commun.* **2009**, 371. (b) Michelet, V.; Toullec, P. Y.; Genét, J.-P. *Angew. Chem., Int. Ed.* **2008**, *47*, 4268. (c) Fürstner, A.; Davies, P. W. *Angew. Chem., Int. Ed.* **2007**, *46*, 3410. (d) Jiménez-Núñez, E.; Echavarren, A. M. *Chem. Commun.* **2007**, 333. (e) Hashmi, A. S. K. *Chem. Rev.* **2007**, *107*, 3180. (f) Marco-Contelles, J.; Soriano, E. *Chem.—Eur. J.* **2007**, *13*, 1350. (g) Marion, N.; Nolan, S. P. *Angew. Chem., Int. Ed.* **2007**, *46*, 2750. (h) Zhang, L.; Sunm, J.; Kozmin, S. A. *Adv. Synth. Catal.* **2006**, *348*, 2271. (i) Bruneau, C. *Angew. Chem., Int. Ed.* **2005**, *44*, 2328. (j) Añobe, L.; Domínguez, G.; Pérez-Castells, J. *Chem.—Eur. J.* **2004**, *10*, 4938. (k) Diver, S. T.; Giessert, A. J. *Chem. Rev.* **2004**, *104*, 1317. (l) Lloyd-Jones, G. C. *Org. Biomol. Chem.* **2003**, *1*, 215. (m) Auber, C.; Buisine, O.; Malacria, M. *Chem. Rev.* **2002**, *102*, 813.

(2) For selected recent examples of 1,6-enyne cycloisomerizations and applications, see: (a) Camelio, A. M.; Barton, T.; Guo, F.; Shaw, T.; Siegel, D. *Org. Lett.* **2011**, *13*, 1517. (b) Jin, T.; Himuro, M.; Yamamoto, Y. *J. Am. Chem. Soc.* **2010**, *132*, 5590. (c) Sylvester, K. T.; Chirik, P. J. *J. Am. Chem. Soc.* **2009**, *131*, 8772. (d) Chung, C.-P.; Chen, C.-C.; Lin, Y.-C.; Liu, Y.-H.; Wang, Y. *J. Am. Chem. Soc.* **2009**, *131*, 18366. (e) Ota, K.; Lee, S. I.; Tang, J.-M.; Takachi, M.; Nakai, H.; Morimoto, T.; Sakurai, H.; Kataoka, K.; Chatani, N. *J. Am. Chem. Soc.* **2009**, *131*, 15203.

(3) For Ag-catalyzed type-I cycloisomerization of enynes, see: Porcel, S.; Echavarren, A. M. *Angew. Chem., Int. Ed.* **2007**, *46*, 2672.

(4) For Au-catalyzed type-I, II, and III cycloisomerizations of enynes, see: (a) Nieto-Oberhuber, C.; Muñoz, M. P.; Buñuel, E.; Nevado, C.; Cárdenas, D. J.; Echavarren, A. M. *Angew. Chem., Int. Ed.* **2004**, *43*, 2402. (b) Jiménez-Núñez, E.; Claverie, C. K.; Bour, C.; Cárdenas, D. J.; Echavarren, A. *Angew. Chem., Int. Ed.* **2008**, *47*, 7892. (c) Bartolomé, C.; Ramiro, Z.; Pérez-Galán, P.; Bour, C.; Raducan, M.; Echavarren, A. M.; Espinet, P. *Inorg. Chem.* **2008**, *47*, 11391. (d) Nieto-Oberhuber, C.; Muñoz, M. P.; López, S.; Jiménez-Núñez, E.; Nevado, C.; Herrero-Gómez, E.; Raducan, M.; Echavarren, A. *Chem.—Eur. J.* **2006**, *12*, 1677.

(5) For Ga-catalyzed type-I cycloisomerization of enynes, see: Inoue, H.; Kotsuma, T.; Murai, S.; Chatani, N. *J. Am. Chem. Soc.* **2002**, *124*, 10294.

(6) In-catalyzed type-I, II, and III cycloisomerizations of enynes: for 1,6-enynes with internal alkynes, type II products were obtained, see: (a) Miyanohana, Y.; Chatani, N. *Org. Lett.* **2006**, *8*, 2155. For 1,6-enyne with a terminal alkyne, type-I product was obtained, see: (b) Nakai, H.; Chatani, N. *Chem. Lett.* **2007**, *36*, 1494.

(7) For Ir-catalyzed type-I and II cycloisomerizations of enynes, see: Inoue, H.; Morimoto, T.; Muto, T.; Murai, S.; Chatani, N. *J. Org. Chem.* **2001**, *66*, 4433.

(8) For Pd-catalyzed type-I and II cycloisomerizations of enynes, see: (a) Trost, B. M.; Tanoury, G. J. *J. Am. Chem. Soc.* **1988**, *110*, 1636. (b) Trost, B. M.; Tour, J. M. *J. Am. Chem. Soc.* **1987**, *109*, 4753.

(9) For Pt-catalyzed type-I cycloisomerization of enynes, see: (a) Miyanohana, Y.; Inoue, H.; Chatani, N. *J. Org. Chem.* **2004**, *69*, 8541. (type-II): (b) Tsukamoto, I.; Miyano, S.; Inoue, Y.; Oi, S. *Organometallics* **2001**, *20*, 3704. (Both type-I and type-II): (c) Furukawa, N.; Sakurai, H.; Murai, S.; Chatani, N. *Organometallics* **1996**, *15*, 901. (d) Ferrer, C.; Raducan, M.; Nevado, C.; Claverie, C. K.; Echavarren, A. M. *Tetrahedron* **2007**, *63*, 6306. (e) Stelzer, F.; Szillat, H.; Fürstner, A. *J. Am. Chem. Soc.* **2001**, *123*, 11863. (f) Fürstner, A.; Szillat, H.; Gabor, B.; Mynott, R. *J. Am. Chem. Soc.* **1998**, *120*, 8305. (g) Fürstner, A.; Szillat, H.; Stelzer, F. *J. Am. Chem. Soc.* **2000**, *122*, 6785.

(10) For Rh-catalyzed type-I and II cycloisomerzations of enynes, see: (a) Ota, K.; Lee, S. I.; Tang, J.-M.; Takachi, M.; Nakai, H.; Morimoto, T.; Sakurai, H.; Kataoka, K.; Chatani, N. *J. Am. Chem. Soc.* **2001**, *131*, 15203. (b) Ota, K.; Chatani, N. *Chem. Commun.* **2008**, 2906.

(11) For Ru-catalyzed cycloisomerizations of enynes, see: (a) Morimoto, T.; Muto, T.; Murai, S.; Chatani, N. *J. Am. Chem. Soc.* **1994**, *116*, 6049. (b) Faller, J. W.; Fontaine, P. P. *J. Organomet. Chem.* **2006**, *691*, 1912.

(12) Zhuo, L.-G.; Zhang, J.-J.; Yu, Z.-X. *J. Org. Chem.* **2012**, *77*, 8527. For convenience in discussing and comparing different model reactions *a-d* in Scheme 3, we have included the computed energy surface of reaction *a* shown in the original *J. Org. Chem.* paper in the present manuscript as Figure 1.

(13) For selected examples of DFT studies of 1, *n*-enyne cycloisomerizations, see: (a) Obradors, C.; Echavarren, A. M. *Acc. Chem. Res.* **2014**, *47*, 902. (b) Soriano, E.; Marco-Contelles, J. *Acc. Chem. Res.* **2009**, *42*, 1026. (c) Cabello, N.; Jiménez-Núñez, E.; Buñuel, E.; Cárdenas, D. J.; Echavarren, A. M. *Eur. J. Org. Chem.* **2007**, 4217. (d) Nieto-Oberhuber, C.; Muñoz, M. P.; López, S.; Cárdenas, D. J.; Buñuel, E.; Nevado, C.; Echavarren, A. M. *Angew. Chem., Int. Ed.* **2005**, *44*, 6146. (e) Soriano, E.; Ballesteros, P.; Marco-Contelles, J. *Organometallics* **2005**, *24*, 3172. (f) Soriano, E.; Ballesteros, P.; Marco-Contelles, J. *Organometallics* **2005**, *24*, 3182. (g) Soriano, E.; Marco-Contelles, J. *J. Org. Chem.* **2005**, *70*, 9345. (h) Soriano, E.; Ballesteros, P.; Marco-Contelles, J. *J. Org. Chem.* **2004**, *69*, 8018. (i) Cabello, N.; Jiménez-Núñez, E.; Buñuel, E.; Cárdenas, D. J.; Echavarren, A. M. *Eur. J. Org. Chem.* **2007**, 4217. (j) Xu, K. L.; Wu, Y.; Xie, D. Q.; Yan, G. S. *Chin. Sci. Bull.* **2004**, *49*, 883.

(14) In the reaction system, the real catalytic species, $InCl_2^+$, will coordinate to the substrate. It is known that In(III) prefers to be tetracoordinated. In our calculations, we considered all stationary points (intermediates, transition states, et al.) to be four-coordinated; therefore, for some stationary points in which In is not coordinationally saturated, we added a solvent molecule as the fourth coordination ligand. When the reactions were carried out in toluene (reactions 2 and 3, Scheme 3), to model toluene, we used a benzene molecule as the explicit solvent molecule, using $\mathbf{InCl_2(benzene)^+}$ as the catalytic species. For reactions carried out in DCE solvent, $\mathbf{InCl_2(DCE)^+}$ was used in the calculations.

(15) (a) The homoallylic cation rearrangement process has also been proposed by Fürstner in their $PtCl_2$-catalyzed enyne isomerization (see refs 9f, g). Tantillo and co-workers have reported a series of non-classic carbocation rearrangements, see: (b) Davis, R. L.; Leverett, C. A.; Romo, D.; Tantillo, D. J. *J. Org. Chem.* **2011**, *76*, 7167. (c) Hong, Y. J.; Tantillo, D. J. *J. Am. Chem. Soc.* **2009**, *131*, 7999. (d) Hong, Y. J.; Tantillo, D. J. *Org. Lett.* **2011**, *13*, 1294. (e) Hong, Y. J.; Tantillo, D. J. *J. Am. Chem. Soc.* **2011**, *133*, 18249.

(16) Frisch, M. J.; Trucks, G. W.; Schlegel, H. B.; Scuseria, G. E.; Robb, M. A.; Cheeseman, J. R.; Scalmani, G.; Barone, V.; Mennucci, B.; Petersson, G. A.; Nakatsuji, H.; Caricato, M.; Li, X.; Hratchian, H. P.; Izmaylov, A. F.; Bloino, J.; Zheng, G.; Sonnenberg, J. L.; Hada, M.; Ehara, M.; Toyota, K.; Fukuda, R.; Hasegawa, J.; Ishida, M.; Nakajima, T.; Honda, Y.; Kitao, O.; Nakai, H.; Vreven, T.; Montgomery, J. A., Jr.; Peralta, J. E.; Ogliaro, F.; Bearpark, M.; Heyd, J. J.; Brothers, E.; Kudin, K. N.; Staroverov, V. N.; Kobayashi, R.; Normand, J.; Raghavachari, K.; Rendell, A.; Burant, J. C.; Iyengar, S. S.; Tomasi, J.; Cossi, M.; Rega, N.; Millam, J. M.; Klene, M.; Knox, J. E.; Cross, J. B.; Bakken, V.; Adamo, C.; Jaramillo, J.; Gomperts, R.; Stratmann, R. E.; Yazyev, O.; Austin, A. J.; Cammi, R.; Pomelli, C.; Ochterski, J. W.; Martin, R. L.; Morokuma, K.; Zakrzewski, V. G.; Voth, G. A.; Salvador, P.; Dannenberg, J. J.; Dapprich, S.; Daniels, A. D.; Farkas, O.; Foresman, J. B.; Ortiz, J. V.; Cioslowski, J.; Fox, D. J. *Gaussian 09*, revision A.02; Gaussian, Inc.: Wallingford, CT, 2009.

(17) (a) Becke, A. D. *J. Chem. Phys.* **1993**, *98*, 5648. (b) Lee, C.; Yang, W.; Parr, R. G. *Phys. Rev. B* **1988**, *37*, 785.

(18) (a) Hay, P. J.; Wadt, W. R. *J. Chem. Phys.* **1985**, *82*, 299. (b) Dunning, T. H., Jr.; Hay, P. J. In *Modern Theoretical Chemistry*; Schaefer, H. F., III, Ed.; Plenum Press: New York, 1977; pp 1−28.

(19) Hehre, W. J.; Radom, L.; Schleyer, P. V. R.; Pople, J. A. *Ab Initio Molecular Orbital Theory*; Wiley: New York, 1986.

(20) (a) Fukui, K. *J. Phys. Chem.* **1970**, *74*, 4161. (b) Gonzalez, C.; Schlegel, H. B. *J. Chem. Phys.* **1989**, *90*, 2154. (c) Gonzalez, C.; Schlegel, H. B. *J. Phys. Chem.* **1990**, *94*, 5523.

(21) (a) Barone, V.; Cossi, M. *J. Phys. Chem. A* **1998**, *102*, 1995. (b) Cossi, M.; Rega, N.; Scalmani, G.; Barone, V. *J. Comput. Chem.* **2003**, *24*, 669. (c) Takano, Y.; Houk, K. N. *J. Chem. Theory Comput.* **2005**, *1*, 70.

(22) HMQC (in the Supporting Information) indicated that the ^{13}C NMR signals of the two Me groups (one in the diene part, one in the Pr group) in **d2-2** overlapped at 13.9 ppm. This event could also have happened in the ^{13}C NMR of **d2-2′**.